Chemical Engineering Science 208 (2019) 115143

Contents lists available at ScienceDirect

Chemical Engineering Science

journal homepage: www.elsevier.com/locate/ces

Effects of functionalization on the performance of metal-organic frameworks for adsorption-driven heat pumps by molecular simulations

Guoqing Hu, Wei Li, Song Li *

State Key Laboratory of Coal Combustion, School of Energy and Power Engineering, Huazhong University of Science and Technology, Wuhan 430074, Hubei, China
Nano Interface Centre for Energy, School of Energy and Power Engineering, Huazhong University of Science and Technology, 430074, China

HIGHLIGHTS

- Functionalization cannot always enhance the uptakes of MOFs.
- Functionalization reduced the COP_C of MOFs with relatively small pores.
- $-NH_2$ functionalization increased the COP_C of MOFs with hierarchical pores.

GRAPHICAL ABSTRACT

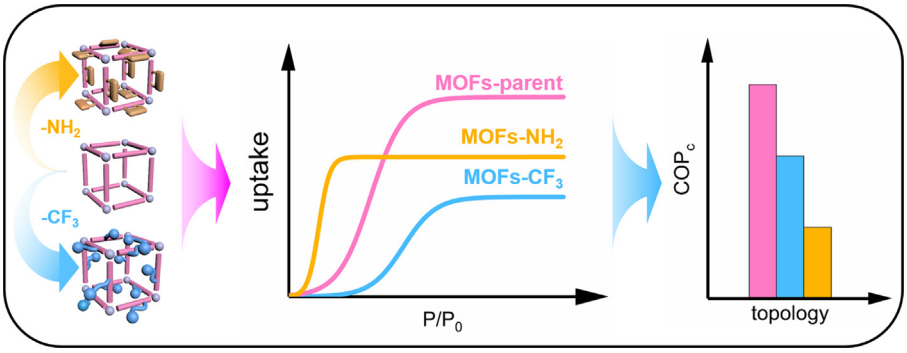

ARTICLE INFO

Article history:
Received 2 May 2019
Received in revised form 18 July 2019
Accepted 2 August 2019
Available online 3 August 2019

Keywords:
Functionalization
Adsorption
Ethanol
Hierarchical pores
Coefficient of performance

ABSTRACT

Metal-organic frameworks (MOFs) are promising adsorbents for adsorption-driven heat pumps (AHPs) due to their outstanding adsorption performance. However, the role of functionality in tuning the AHP performance has not been elucidated. In this work, the ethanol adsorption behaviors and AHP performance of Zr-based MOFs in three topologies (i.e. *csq*, *ftw* and *scu*) functionalized by $-NH_2$ and $-CF_3$ exhibiting different affinities towards ethanol working fluid were investigated by grand canonical Monte Carlo simulations (GCMC). It was revealed that functionalization not only affected the adsorption capacity but also shifted the steps of isotherms to the low pressure upon functionalization by $-NH_2$. *scu*-MOFs exhibited the higher coefficient of performance for cooling (COP_C) than *csq*-MOFs and *ftw*-MOFs. Moreover, functionalization reduced the COP_C of *ftw*-MOFs and *scu*-MOFs due to the lower working capacity resulting from the reduced pore volumes. On the contrary, the COP_C of *csq*-MOFs can be improved upon functionalization by $-NH_2$.

1. Introduction

Nowadays, approximately 45% of the building energy consumption is used for cooling and heating (Berry, 2015). The electricity consumption resulting from cooling and heating demand is expected to increase by ten times from 2010 to 2100 because of more severe global warming (Clarke et al., 2018). Thus, to reduce the electricity cost and greenhouse effects, the development of energy-saving heat pumps for cooling and heating has been proposed. Compared with conventional compression-based heat pumps, the adsorption-driven heat pumps (AHPs) powered by low-grade heat sources (e.g. industrial waste heat and solar energy) are attracting growing attention (Henning, 2007). However, the coefficient of performance (COP) of AHPs, that is closely related to the working capacity (ΔW) and average enthalpy of

* Corresponding author.
E-mail address: songli@hust.edu.cn (S. Li).

https://doi.org/10.1016/j.ces.2019.08.001
0009-2509/

adsorption ($\langle\Delta_{ads}H\rangle$) (Li et al., 2019), is generally lower compared to the conventional compression-based heat pumps. The conventional adsorbents (e.g. zeolites, activated carbons and silica gel) usually display mediocre adsorption capacity and/or extremely high enthalpy of adsorption which cannot meet the requirements for high-performing AHPs (de Lange et al., 2015; Demir et al., 2008). One effective approach to improve COP of AHPs is developing novel adsorbents with superior adsorption performance.

Metal-organic frameworks (MOFs) assembled by metal nodes and organic ligands are considered as the most promising adsorbents due to their ultra-large accessible surface area (ASA) (Zhou et al., 2012). The adsorption capacity of working fluids (i.e. alcohols and water) on MOFs of AHPs has been reported. Rezk *et al.* investigated the ethanol adsorption characteristics of six MOFs including MIL-101Cr, MIL-53Cr, MIL-100Cr, CPO-27Ni, Cu-BTC and Fe-BTC, all of which exhibited the higher ethanol uptake than the commercial silica gel (0.2 g/g) at 298 K. Among all MOFs, MIL-101Cr exhibited the highest ethanol uptake up to 1.2 g/g (Rezk et al., 2013). Therefore, MIL-101Cr was one of the most promising MOFs for cooling/heating (Henninger et al., 2012; Rezk et al., 2013). Henninger *et al.* reported a novel MOF (i.e. ISE-1) that exhibited the higher water loading spread (0.21 g/g) over one cooling cycle than commercial silica gel and zeolites (Henninger et al., 2009). Benjamin *et al.* also reported that Al-based MOFs outperformed the zeolites in water adsorption performance (Benjamin and Chakraborty, 2018).

Given the structure tunability of MOFs (Lin et al., 2012), many studies make efforts to improve their adsorption performance by tuning the surface chemistry using functionalization. The water adsorption performance of MIL-101–X containing different functional groups (X = –H, $–NO_2$, $–NH_2$ and $–SO_3H$) were experimentally investigated, in which the water uptake of MIL-101 was reduced upon functionalization regardless of functional group (Akiyama et al., 2012). Meanwhile, the shape of water adsorption isotherms can be tuned by introducing functional groups with different hydrophilicities (Akiyama et al., 2012). Similarly, Zn-NDI-X with different functional groups (X = –H, –NHEt and –SEt) also exhibited decreased water uptakes compared with pristine Zn-NDI–H. However, when the hydrophobic functional group –SEt was replaced with more hydrophilic ethyl sulfoxide or ethyl sulfone, the water uptake was remarkably improved, indicating that increasing hydrophilicity of MOFs may favor their water adsorption (Wade et al., 2013). Moreover, aminated MIL-101Cr–NH_2 was also reported to exhibit the higher water uptake than parent structure and remained high water stability after 40 adsorption/desorption cycles (Khutia et al., 2013).

On the other hand, the shape of adsorption isotherm or step position is another important factor influencing the COP of AHPs. According to the previous works (Aristov, 2013; Glaznev et al., 2009; Okunev et al., 2013), the stepwise adsorption isotherm or "S" shaped isotherm is beneficial for the thermodynamic and dynamic adsorption performance of AHPs on account of a small change in pressure leading to the large variation in uptake. Glaznev *et al.* reported type V adsorption isotherm with a step position of P/P_0 = 0.05–0.4 was favorable for the COP of AHPs (Glaznev et al., 2009). It has been reported that amino groups were commonly introduced into MOFs to enhance the interaction strength between adsorbate and MOFs (Sumida et al., 2011), thus leading to the shift of adsorption isotherms. It was found that the introduced hydrophilic amino group into MOFs (i.e. UiO-66) may shift the step position to the lower P/P_0 of water adsorption isotherm (Jeremias et al., 2013). It was also demonstrated that the step of water adsorption isotherm for MIL-125–NH_2 was located at approximately P/P_0 = 0.2, which is favorable for AHP performance (Jeremias et al., 2013). In addition, the effects of functional groups with different hydrophilicities ($–NO_2$, $–NH_2$ and $–SO_3H$) on the water adsorption behavior of MIL-101 were investigated (Akiyama et al., 2012), in which the steps of the adsorption isotherms of MIL-101–NH_2 and MIL-101–SO_3H were shifted to the low P/P_0 compared with that of MIL-101, suggesting that the critical role of hydrophilic functional groups in tuning the steps of adsorption isotherms. On the contrary, the isotherm shape of MIL-101–NO_2 was almost identical to MIL-101, which was attributed to the relatively weak hydrophilicity of $–NO_2$ (Akiyama et al., 2012).

Although many experimental studies reported the importance of functionalization on the adsorption behaviors of MOFs, the influence of functional modifications on adsorption and cooling performance of MOFs for ethanol-based AHPs, especially the relationship between functionalization and cooling performance, has not been elucidated. To explore the effects of functional groups with varying affinities on ethanol adsorption behaviors as well as the coefficient of performance for cooling (COP_C) of MOF-based AHPs, we modified Zr-based MOFs of three topologies (i.e. *csq*, *ftw* and *scu*) with hydrophilic $–NH_2$ and relatively hydrophobic $–CF_3$. Then, we investigated their ethanol adsorption and cooling performance by grand canonical Monte Carlo (GCMC) simulations. This study may provide insights into developing and designing high-performing MOFs for AHPs by post-synthetic modifications.

2. Methodology

2.1. MOF structure

In this work, all the structures were chosen from Zr-based MOFs owing to their excellent stability. In order to exclude the influence from the type of metal node and linkers, all MOFs consist of identical Zr-based metal node and organic linker (Bai et al., 2016). In detail, the primary Zr-MOFs were built by the Secondary Building Units (SBUs, Zr_6O_4) (Fig. 1d) and the organic linker, i.e. benzene-1,2,4,5-propiolic acid (p4t), (Fig. 1e), which were assembled into MOFs of three topologies: *csq* (Fig. 1a), *ftw* (Fig. 1b) and *scu* (Fig. 1c). Two types of functional groups, amino ($–NH_2$) and trifluoromethyl ($–CF_3$) were chosen as the representative functional groups exhibiting different affinities towards ethanol (Banerjee et al., 2011; Serre, 2012). Each linker was functionalized at the remaining –H sites of the organic linker by one type of functional group ($–NH_2$ or $–CF_3$) as shown in Fig. 1e. The functional group modification and geometric optimization of MOFs were performed in Forcite module of Materials Studio (Segall et al., 2002), followed by structure optimization in VASP (Hafner, 2008). The accessible surface area (ASA) of all MOFs was computed from RASPA 1.9 (Dubbeldam et al., 2016). The largest cavity diameter (LCD), and available pore volume (V_a) were obtained from Zeo++0.3 (Willems et al., 2012) using the nitrogen probe with a radius of 1.86 Å.

2.2. Coefficient of performance for cooling (COP_C) calculation

The COP_C was calculated based on the basic thermodynamic cycle of AHPs according to Eq. (1) reported in our previous work (Li et al., 2019).

$$COP_c = \frac{\Delta_{vap}H\rho_{liq}^{wf}m_{sorbent}\Delta W}{\rho_{liq}^{wf}\langle\Delta_{ads}H\rangle\Delta W - M_W C_p^{sorbent}(T_{des}-T_{con})} \quad (1)$$

Here, $\Delta_{vap}H$ was the evaporation enthalpy of ethanol at evaporation temperature (T_{ev}) obtained from NIST (Majer et al., 1985).ρ_{lip}^{wf} = 0.75 g/cm^3, which was the average density of ethanol between 308 K and 358 K. $m_{sorbent}$ was the mass of the adsorbent. $C_p^{sorbent}$ was the heat of capacity of MOF adsorbents, which is 1 J/(g·K) according to previous study (de Lange et al., 2015). ΔW

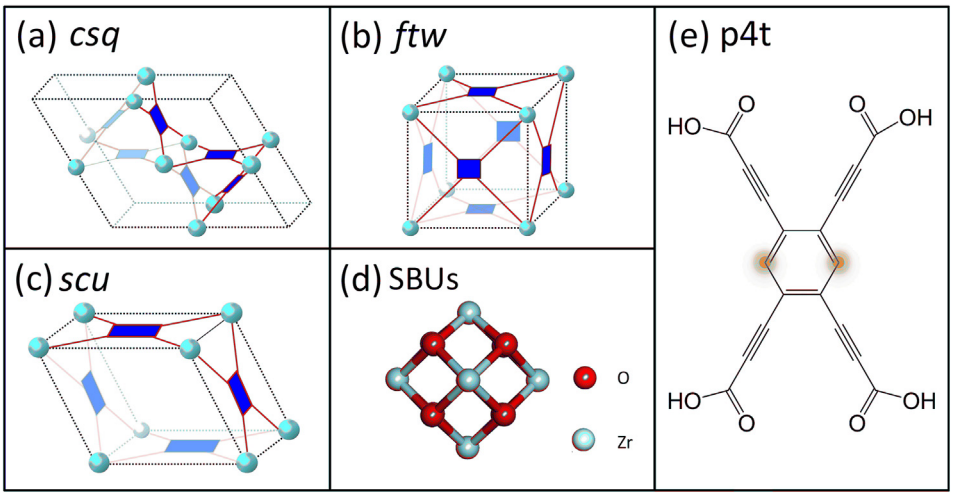

Fig. 1. Zr-MOFs in (a) *csq*, (b) *ftw* and (c) *scu* topology composed of the (d) metal node and (e) organic linker. The sites highlighted in orange refer to the sites functionalized by $-CF_3$ or $-NH_2$. (For interpretation of the references to colour in this figure legend, the reader is referred to the web version of this article.)

was the working capacity between maximum adsorption capacity of adsorption stage (from IV to I in Fig. 2) and minimum adsorption capacity of desorption stage (from II to III in Fig. 2). M_W = 46 g/mol was the molar mass of the adsorbate and $\langle \Delta_{ads}H \rangle$ was the average enthalpy of adsorption during the thermodynamical cycle of AHPs (Eq. (2)).

$$\langle \Delta_{ads}H \rangle = \frac{\int_{W_{\min}}^{W_{\max}} \Delta_{ads}H(W)dW}{W_{\max} - W_{\min}} \tag{2}$$

In this work, we chose the typical cooling operating conditions of AHPs, in which evaporation temperature T_{ev} = 285 K, condensation temperature T_{con} = 300 K, adsorption temperature T_{ads} = 308 K and desorption temperature T_{des} = 358 K. Considering the low-grade heat sources (<373 K, e.g., waste heat, solar energy) (Henning, 2007), the desorption temperature T_{des} = 358 K was employed. Corresponding to the operation temperatures, the saturation pressures of ethanol at evaporation temperature and condensation temperature were P_{ev} = 3420 Pa and P_{con} = 8200 Pa, respectively. Thus, GCMC simulations were performed at the corresponding conditions, i.e. stage I (T_{ads} = 308 K, P_{ev} = 3420 Pa), stage II (T_{II} = 328 K, P_{con} = 8200 Pa) and stage III (T_{des} = 358 K, P_{con} = 8200 Pa) (Fig. 2) to obtain the ethanol working capacity (ΔW) and average enthalpy of adsorption ($\langle \Delta_{ads}H \rangle$) for COP_C.

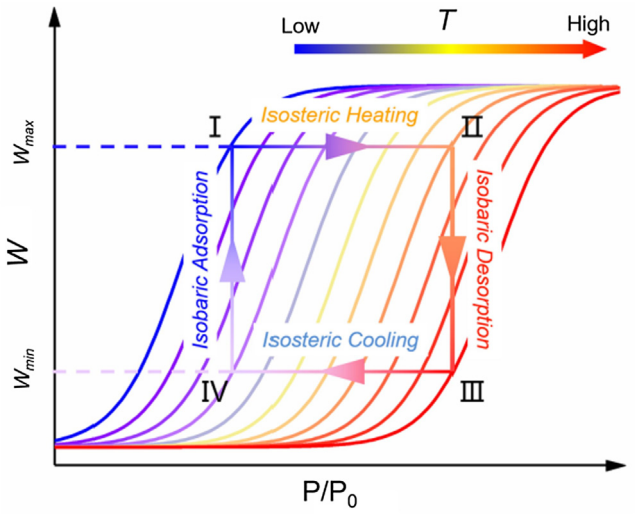

Fig. 2. Basic thermodynamic cycles for adsorption-driven heat pumps.

2.3. Simulation details

The electrostatic surface potential computed by plane-wave density functional theory (DFT) with VASP (Hafner, 2008) was fitted by the density derived electrostatic and chemical (DDEC) method to obtain the atomic partial charges of MOFs. The energy cutoff of electronic relaxation was 450 eV and the Brillouin zone sampling region was in a 1 × 1 × 1 Monkhorst-Pack k-point mesh. The non-bonded interactions between MOFs and adsorbates were described by the Lennard-Jones (LJ) and Coulomb potentials, as shown in Eq. (3).

$$U_{ij} = 4\varepsilon_{ij}\left[\left(\frac{\sigma_{ij}}{r_{ij}}\right)^{12} - \left(\frac{\sigma_{ij}}{r_{ij}}\right)^{6}\right] + \frac{q_i q_j}{4\pi\varepsilon_0 r_{ij}} \tag{3}$$

Herein, i and j represented the interacting particle of the adsorbate or MOFs. ε_{ij} was the depth of the well potential and σ_{ij} was the van der Waals distance, which were taken from the Universal Force Field (UFF) (Rappé et al., 1992) as shown in Table S1 of Supporting Information (SI). r_{ij} was the distance between two atoms. q_i and q_j were the partial charges of atoms. The LJ parameters and partial charges of ethanol were obtained from Transferable Potentials for Phase Equilibria (TraPPE) force field (Table S2) (Potoff and Siepmann, 2001), which has been validated for describing the ethanol adsorption in previous studies(Erdős et al., 2018; Nalaparaju et al., 2010; Wang et al., 2014). Lorentz-Berthelot mixing rule was used to obtain the LJ parameters between different atom types. The Ewald method was applied for the electrostatic interaction with a cutoff of 12.8 Å. Grand canonical Monte Carlo simulations (GCMC) were performed in RASPA 1.9 (Dubbeldam et al., 2016) to obtain the working capacity, enthalpy of adsorption and interaction energy. 1.5×10^6 Monte Carlo cycles consisting of 0.5×10^6 initialization cycles to initialize the system and 1×10^6 cycles for the production run for each system. Monte Carlo moves including random insertion, deletion, translation and rotation with the identical probability were applied. All the simulations were performed at temperatures ranging from 308 K to 358 K below the ethanol saturated vapor pressure of 308 K (13.6 kPa).

3. Results and discussion

3.1. Ethanol adsorption performance

The structure properties of all the MOFs including LCD, ASA and V_a were shown in Table 1 and Fig. 3. Among all the MOFs, *csq*-MOFs

Table 1
The largest cavity diameter (LCD), available pore volume (V_a) and accessible surface area (ASA) of MOFs.

Topology	Functional group	LCD (Å)	V_a (m^3/g)	ASA (m^2/g)
csq	parent	23.90	0.91	1885
	$-CF_3$	24.00	0.67	1482
	$-NH_2$	23.90	0.84	1671
ftw	parent	10.58	0.48	1937
	$-CF_3$	8.08	0.24	1082
	$-NH_2$	10.57	0.37	1482
scu	parent	9.02	0.59	1942
	$-CF_3$	9.22	0.39	1498
	$-NH_2$	9.02	0.53	1692

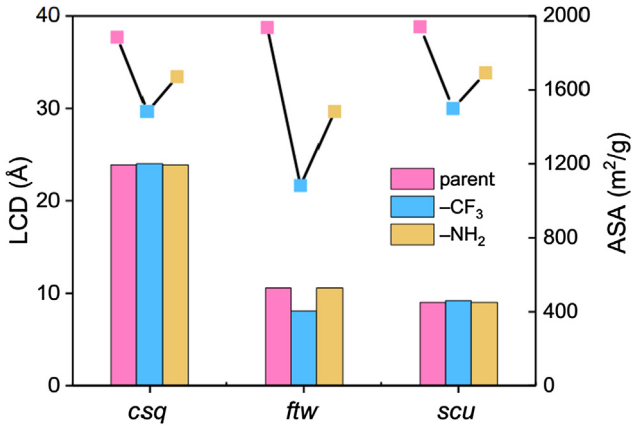

Fig. 3. The LCD (columns) and ASA (symbols) of MOFs in three topologies with different functional groups.

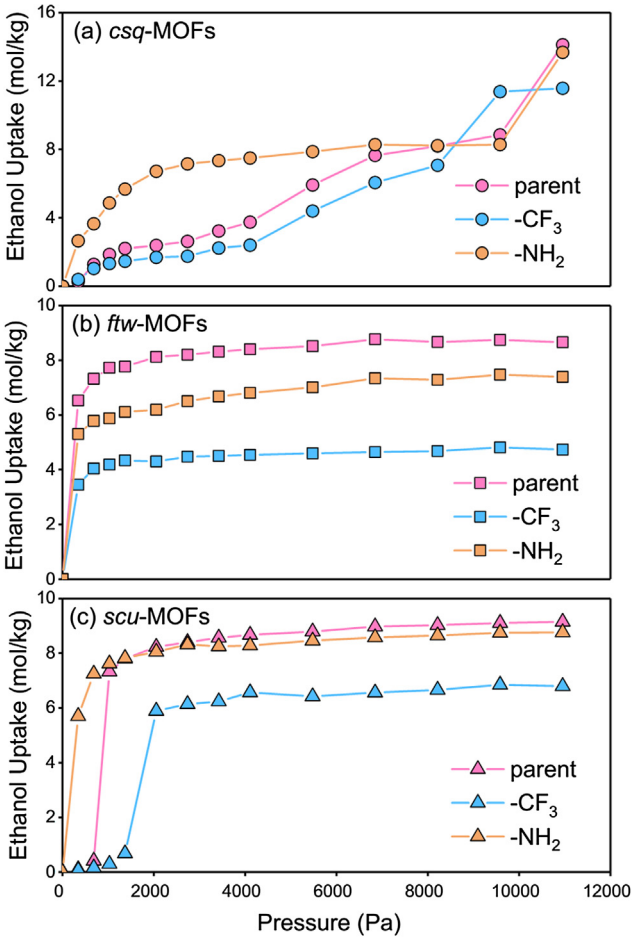

Fig. 4. The ethanol adsorption isotherms of (a) *csq*-MOFs, (b) *ftw*-MOFs and (c) *scu*-MOFs modified by different functional groups at 308 K.

displayed the largest LCD followed by *ftw*-MOFs and *scu*-MOFs regardless of the functionalization (Fig. 3). There is no significant decrease in LCD of MOFs upon functionalization except *ftw*-MOF–CF_3, similar to our previous works (Li and Li, 2018). On the other hand, the introduction of functional groups decreased ASA of all the MOFs, in which MOFs–CF_3 shows the smaller ASA than MOFs–NH_2 due to the larger size of $-CF_3$. The similar tendency was observed in V_a (Fig. S1). The results demonstrated that the functional groups decreased ASA and V_a but not LCD of MOFs.

Adsorption capacity is one of the important criteria evaluating AHP performance. The ethanol adsorption isotherms of MOFs were closely relevant to the topology and functional groups (Fig. 4). Generally, the uptakes of *csq*-MOFs at the highest pressure are higher than *scu*-MOFs and *ftw*-MOFs, consistent with their trend in pore volumes of Fig. S1. Particularly, *scu*-MOFs and *ftw*-MOFs exhibited similar trend, in which unfunctionalized MOFs–parent possessed the highest adsorption capacity followed by the MOFs–NH_2 and MOFs–CF_3 (Fig. 4b and c) due to the reduced pore volume in the presence of functional groups. However, the dissimilar trend was found in *csq*-MOFs, in which *csq*-MOFs–NH_2 shown the highest uptake followed by *csq*-MOFs–parent and *csq*-MOFs–CF_3 under a wide range of pressures. Whereas at the highest pressure, *csq*-MOFs–parent exhibited the highest uptake followed by *csq*-MOFs–NH_2 and *csq*-MOFs–CF_3 (Fig. 4a). Such a tendency was ascribed to the hierarchical pores of *csq*-MOFs including both micropores and mesopores (Fig. S2a), in which small micropores were easily saturated at low pressure followed by the filling of relatively large mesopores with the increasing pressure. Therefore, at low pressure, the ethanol adsorption in micropores dominates the uptakes due to the strong interaction strength between micropores and adsorbates, especially for *csq*-MOFs–NH_2. At high pressure, both micropores and mesopores volumes determine the uptakes, resulting in the higher uptake of *csq*-MOFs-parent due to its higher pore volume.

Regarding the impacts of functionalization on the shape of isotherm, the introduction of $-NH_2$ led to a shift in steps of adsorption isotherm to the low pressure of MOFs, and the opposite tendency was observed in MOFs–CF_3, especially for *csq*-MOFs (Fig. 4a) and *scu*-MOFs (Fig. 4c). Such a trend may be mainly resulted from the higher affinity of $-NH_2$ towards ethanol than $-CF_3$, which will be discussed later. *ftw*-MOFs exhibited insignificant tendency in which *ftw*-MOF–parent and *ftw*-MOF–NH_2 shown similar steps, whereas *ftw*-MOF–CF_3 presented a slightly larger steps (Fig. 4b). From the perspective of adsorption isotherm shape, *csq*-MOFs shown an isotherm of multiple steps, implicating the presence of hierarchical pores including both micropores (~7.5 Å, Fig. S2a) and mesopores (~23 Å, Fig. S2a), thus leading to the stepwise filling of adsorbates. *ftw*-MOFs consisting of only micropores shown type I isotherm, suggesting their adsorption saturation can be achieved at relatively low pressures, and thus their ethanol uptake was dominated by the pore volume (V_a). Similarly, the uptake of *scu*-MOFs was also dominated by their pore volume. However, the step of type V isotherm of *scu*-MOF–parent can be tuned to type I-like and type V isotherm upon functionalization, which may be favorable for AHP performance according to previous study on PCN-600 (Chen et al., 2019).

The density distribution maps of ethanol adsorbates in the adsorbents at 308 K and 3420 Pa were computed to further identify the distribution of the ethanol molecules in MOFs (Fig. 5). Apparently, ethanol molecules were preferentially assembled in small

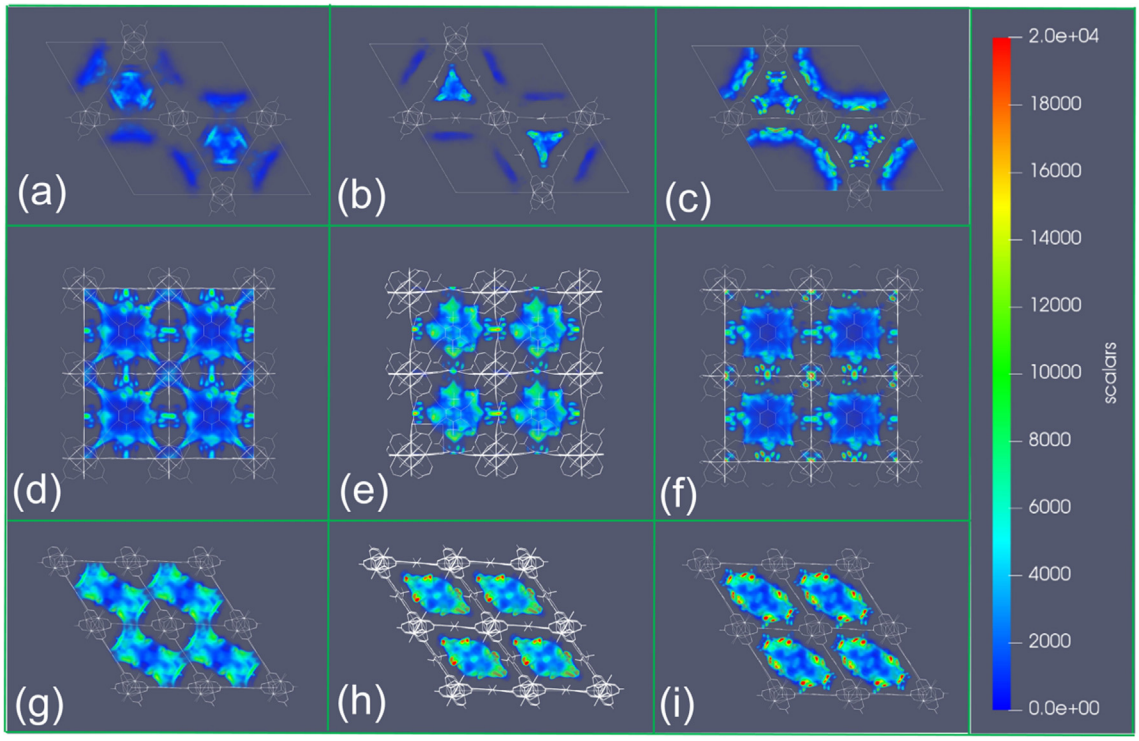

Fig. 5. The density distribution maps of ethanol adsorbates in *csq*-MOFs (a, b, c), *ftw*-MOFs (d, e, f) and *scu*-MOFs (g, h, i) including parent MOFs (a, d, g), and functionalized MOFs by $-CF_3$ (b, e, h) and $-NH_2$ (c, f, i) at 308 K and 3420 Pa.

pores of *csq*-MOFs regardless of modification, and an uptake enhancement in micropores and the surface of mesopores was observed upon functionalized by $-NH_2$ (Fig. 5a–c), consistent with Fig. 4a. The results also demonstrated that *csq*-MOF–NH_2 exhibited the maximum adsorption capacity (Fig. 5c), followed by *csq*-MOF–parent (Fig. 5a) and *csq*-MOF–CF_3 (Fig. 5b). The introduction of $-CF_3$ into *csq*-MOFs increased the ethanol uptake in the microporous but decreased the uptake in the mesopores (Fig. 5b), leading to the overall reduction in uptake as shown in Fig. 4a. For comparison, the adsorption capacity of *csq*-MOFs–NH_2 was increased in not only small pores but also large pores, leading to the increased uptake due to the increased number of adsorption sites provided by $-NH_2$ (Fig. 5c). Compared with the *csq*-MOFs, the ethanol molecules adsorbed in *ftw*-MOFs and *scu*-MOFs were more widely distributed because of their relatively narrow pore size distribution. The ethanol distribution of *ftw*-MOFs was remarkably dependent on the functional groups, which was narrowed down upon functionalization due to the reduced pore volumes. It was also noticed that the fewer ethanol molecules aggregated at the organic linker of *ftw*-MOF–CF_3 (Fig. 5e) while more was observed for *ftw*-MOF–NH_2 (Fig. 5f) compared with *ftw*-MOF–parent (Fig. 5d), which is possibly due to the increased interaction strength between *ftw*-MOF–NH_2 and ethanol. The ethanol distribution of *scu*-MOFs exhibited similar trend with *ftw*-MOFs, in which the increased adsorption sites can be clearly inspected in *scu*-MOFs–NH_2 due to the increased interaction strength between $-NH_2$ and ethanol molecules.

3.2. Interaction energy

According to the above findings, the interaction energy played a crucial role in determining the adsorption behavior and distribution of ethanol molecules. To further demonstrated the adsorption mechanism between the derived MOFs and adsorbate molecules, the host-adsorbate or adsorbate-adsorbate interaction energy were further divided into two parts: electrostatic interaction (Coulombic) and van der Waals interaction energy (VDW) as shown in Fig. 6 for *scu*-MOFs. In general, *ftw*-MOFs exhibited the highest total interaction strength at low P/P_0 (Fig. S4c), followed by *csq*-MOFs (Fig. S3c) and *scu*-MOFs (Fig. 6c) in consistence with their adsorption isotherms, in which the strong interaction implicated type I isotherm for *ftw*-MOFs and the relatively weak interaction energy suggested type V isotherms for *scu*-MOFs. Among all structures, VDW interaction dominated their host-adsorbate interaction, and the adsorbate-adsorbate interaction was mainly determined by Coulombic interaction. Moreover, upon functionalization by $-NH_2$, the Coulombic contribution to host-adsorbate interaction was greatly enhanced for *csq*-MOFs (Fig. S3b) and *scu*-MOFs (Fig. 6b), thus leading to the shift of adsorption steps towards the low P/P_0, which is not evident for *ftw*-MOFs (Fig. S4b). VDW in the MOFs functionalized by $-NH_2$, especially *scu*-MOF–NH_2, slightly decreased under the low relative pressure ($P/P_0 < 0.1$), indicating the role of $-NH_2$ in decreasing VDW and increasing Coulombic interaction. On the contrary, incorporation of $-CF_3$ resulted in the decreased Coulombic interaction, especially in *scu*-MOFs–CF_3 (Fig. 6e). Compared with host-adsorbate interaction energy of MOF–parent, VDW of MOF–CF_3 was increased, especially at low pressure for *csq*-MOF–CF_3 (Fig. S3e) and *scu*-MOF–CF_3 (Fig. 6e), implying the role of $-CF_3$ in enhancing VDW interaction and reducing Coulombic interaction. It was noted that there was no significant variations in the interactions of *ftw*-MOFs (Fig. S4), which is mainly ascribed to the strong host-adsorbate interaction between MOFs and ethanol throughout the pressure range, leading to the negligible contributions of $-NH_2$ and $-CF_3$. Overall, the total interaction energy as a function of pressure of MOFs correlated with the shape of their adsorption isotherms.

To assess the regeneration performance of MOFs for AHPs, the regeneration percentage (R%) at adsorption and desorption or regeneration conditions were calculated based on the adsorption isotherms throughout the operation temperatures for *csq*-MOFs (Fig. S5), *ftw*-MOFs (Fig. S6) and *scu*-MOFs (Fig. S7). Here, R% is defined as the ethanol working capacity (ΔW) divided by the

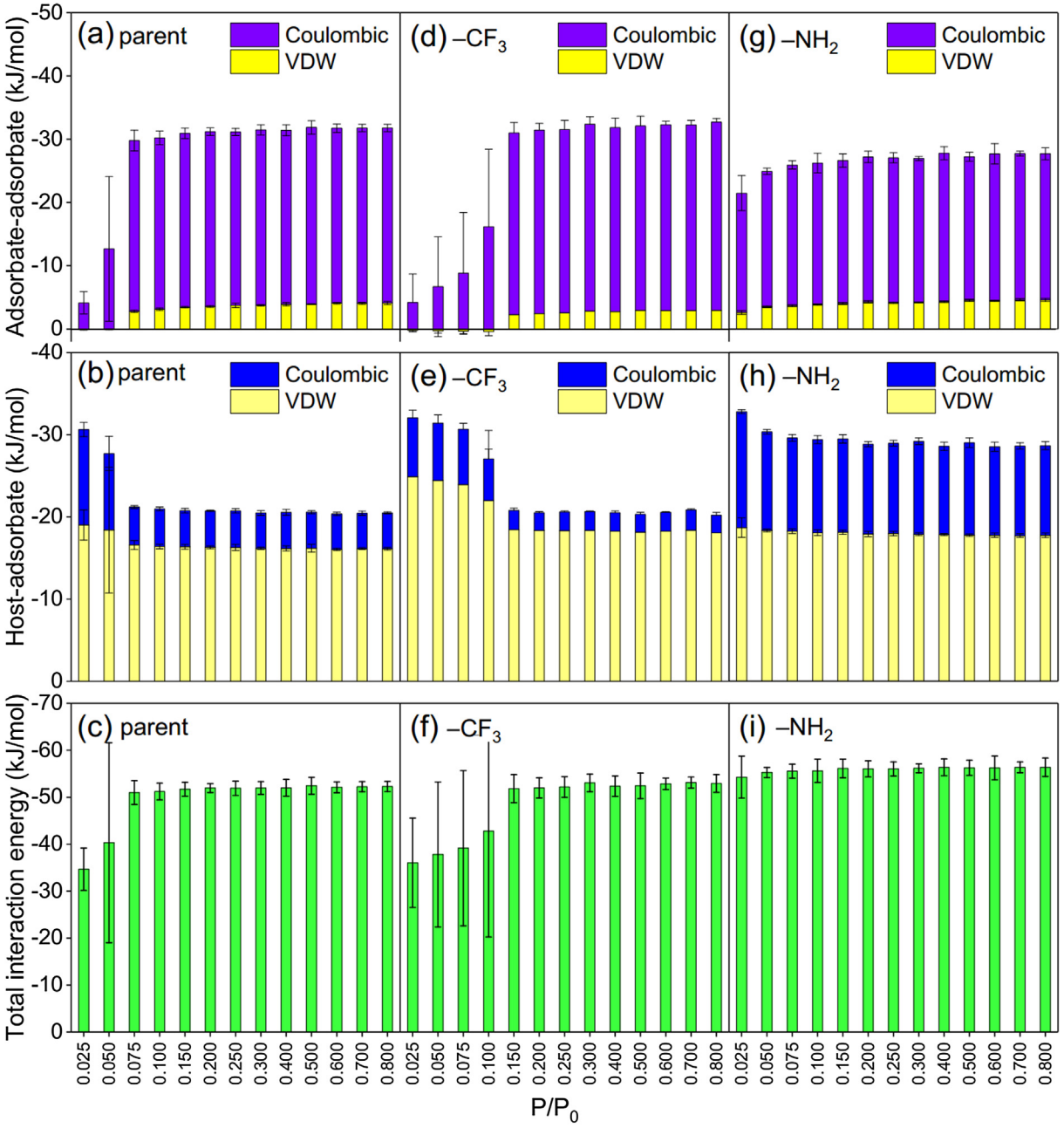

Fig. 6. The interaction energy of (a, d, g) adsorbate-adsorbate, (b, e, h) host-adsorbate and (c, f, i) the total interaction energy of *scu*-MOFs calculated from GCMC simulations at 308 K.

maximum uptake at adsorption condition (stage II of Fig. 2). According to Table S3, R% of *scu*-MOFs is the highest (up to 93%) except *scu*-p4t–NH_2, indicating the outstanding regeneration performance, followed by the *csq*-MOFs and *ftw*-MOFs. Such a tendency corresponded to the total interaction energy between their adsorption (308 K) and desorption temperatures (358 K) for *scu*-MOFs (Fig. 7), *csq*-MOFs (Fig. S8) and *ftw*-MOFs (Fig. S9), which mainly resulted from the compensation between increased Columbic contributions of host-adsorbate and decreased adsorbate-adsorbate interaction (Fig. 7a, b, d and e). Similar tendency was observed for other functionalized MOFs (Figs. S10–15). Consequently, the interaction energy of adsorbate-adsorbate dominated the regeneration performance, in which the larger the difference in interaction energy between adsorption and regeneration conditions, the higher the regeneration performance is.

3.3. Coefficient of performance for cooling

Based on the above obtained ethanol working capacity (ΔW) and average enthalpy of adsorption ($-\langle\Delta_{ads}H\rangle$), The COP_C of different MOFs-based AHPs can be computed as shown in Fig. 8. Consistent with our former analysis, *scu*-MOFs are the most promising candidates for adsorption cooling given their higher COP_C than *csq*-MOFs and *ftw*-MOFs (Fig. 8a). Such a trend is in agreement with their working capacity (Fig. 8b), indicating the dominant role of working capacity in COP_C. However, the COP_C of MOFs upon functionalization is generally decreased in the order: MOF–parent > MOF–CF_3 > MOF–NH_2 due to the reduced working capacity. However, such a tendency is not correlated with the average enthalpy of adsorption ($-\langle\Delta_{ads}H\rangle$), indicating its insignificant role in determining COP_C in these cases. According to our previous work

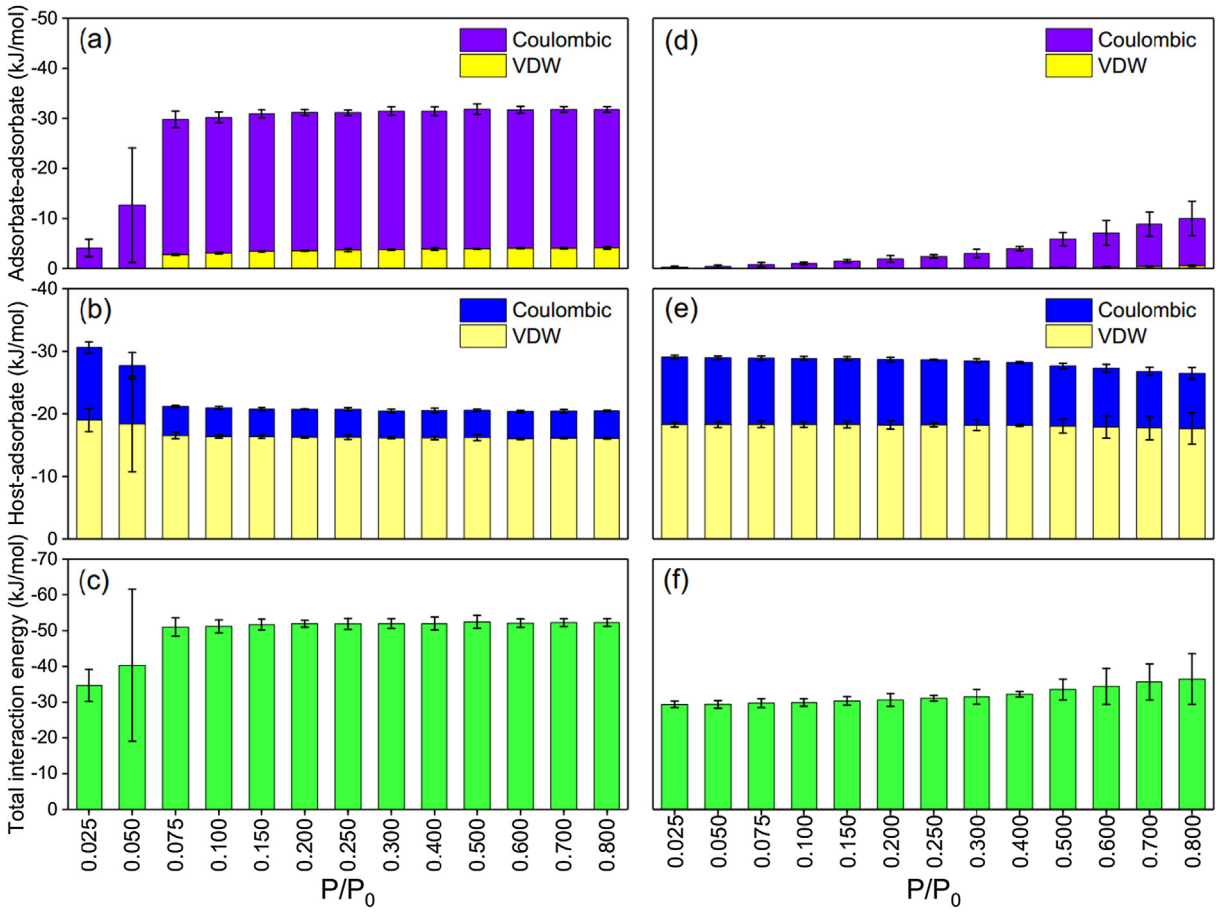

Fig. 7. The interaction energy for *scu*-MOF-parent including (a, d) adsorbate-adsorbate, (b, e) host-adsorbate and (c, f) the total interaction energy calculated from GCMC simulations at (a, b, c) 308 K and (d, e, f) 358 K.

(Li et al., 2019), for MOFs with small, their working capacity played a predominating role in COP_C rather than the average enthalpy of adsorption. In addition, $-NH_2$ modification significantly enhanced the ethanol uptake of *csq*-MOF–parent (Fig. 4a) and the ethanol working capacity at predefined operation condition (Fig. S5c), leading to the higher COP_C. Such different impacts of functionalization on COP_C is mainly ascribed to their discrepancy in working capacity of MOFs in various topology, which may be interpreted from their different structure characteristics. The hierarchical pores of *csq*-MOFs (Fig. S2a) possess extra space for functional groups to provide additional adsorption sites for adsorbates, leading to high working capacity. Similar phenomena have been reported in our previous work on CO_2 adsorption (Li et al., 2017), in which the most significant enhancement in CO_2 uptake of MOFs upon functionalization can only be observed in MOFs with moderate pore sizes. Small pore-sized MOFs can be easily saturated and thus cannot provide sufficient space for extra functional groups; whereas when the pore is too large, functionalization does not impose remarkable enhancement on the uptake due to the small fraction of increased adsorption sites compared with the total space of their parent counterparts. For ethanol adsorption of this work, both *ftw*-MOFs and *scu*-MOFs are small pore-sized MOFs whose uptake cannot be enhanced, leading to the decreased working capacity and COP_C. On the contrary, *csq*-MOF–parent possessing mesopores provides a suitable platform for functionalization, in which functionalization by $-NH_2$ with stronger affinity towards ethanol contributes to the enhanced uptake as well as COP_C. Overall, *scu*-MOFs exhibited the best cooling performance compared with *csq*-MOFs and *ftw*-MOFs due to their high working capacity.

4. Conclusion

In this work, we investigated the effects of functionalization (i.e. $-CF_3$ and $-NH_2$) on adsorption behavior and AHP performance of MOFs of three topologies (*csq*, *ftw* and *scu*) by GCMC simulations. It was found that both working capacity and adsorption isotherm shape were affected by the functionalization. In general, functionalization by either $-CF_3$ or $-NH_2$ reduced the saturated working capacity of *ftw*- and *scu*-MOFs due to the decreased pore volume. The steps of the adsorption isotherms of $-NH_2$ functionalized MOFs generally shifted to the low pressure resulting from the increased interaction strength between $-NH_2$ and ethanol, which was mainly contributed by Coulombic interaction. On the contrary, the working capacity of *csq*-MOFs was remarkably enhanced by $-NH_2$ functionalization, which is mainly due to the hierarchical pores that possess sufficient space for incorporated $-NH_2$ to provide additional adsorption sites for ethanol, which favors the AHP performance. Among all MOFs, *scu*-MOFs exhibited the highest COP_C dominated by their high working capacity. In addition, functionalization does not improve the COP_C of MOFs except *csq*-MOFs, which can be ascribed to the enhanced working capacity resulting from their hierarchical pores. This work demonstrated that functionalization cannot improve the AHP performance of MOFs with small pores, because their adsorption performance and COP_C are dominated by their pore volumes. However, functionalization is favorable for the COP_C of MOFs with hierarchical pores that provides sufficient functionalization space for additional adsorption sites. This work can help understand experimental observations on the reduced uptake of functionalized MOFs and the variation

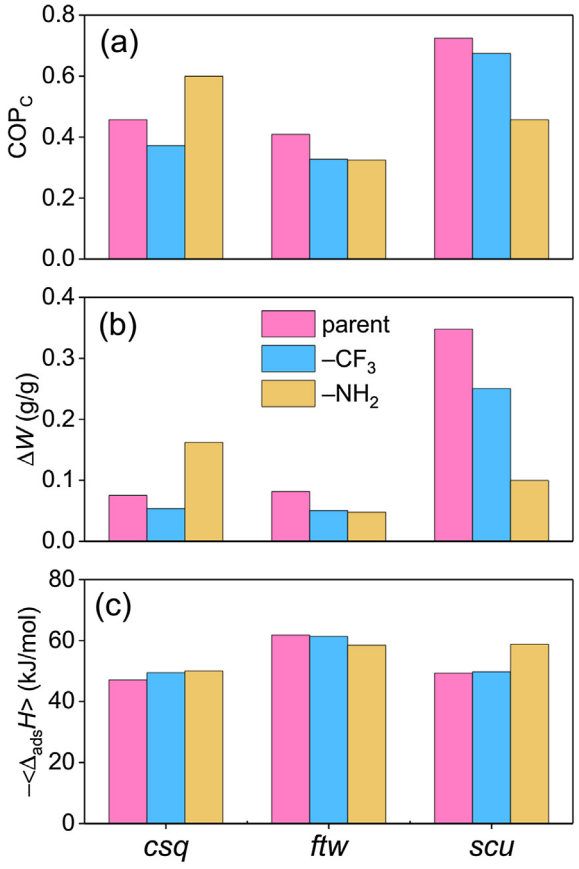

Fig. 8. (a) The coefficient of performance for cool (COP_C), (b) working capacity (ΔW) and (c) averaged enthalpy of adsorption ($-\langle\Delta_{ads}H\rangle$) of MOFs-parent, MOFs–$CF_3$ and MOFs–NH_2.

in their adsorption isotherm shapes. It should be noted that the computational approach reported in this work can be extended to other functional groups as well as adsorbents, which deserves further investigations in future. This work may also provide advanced insights into designing and developing high-performing MOFs for AHPs by functionalization, which may guide both experimental and theoretical exploration in this community. However, the detailed relationship between the functionality property, MOF structure properties, adsorption performance and COP_C requires further investigations in future.

Declaration of Competing Interest

There is no conflict of interest to declare.

Acknowledgement

This work was supported by the National Natural Science Foundation of China (NSFC) under Project No. 51606081 and double first-class research funding of China-EU Institute for Clean and Renewable Energy (No. ICARE-RP-2018-HYDRO-001). This work was carried out at National Su-percomputer Center in Shenzhen.

Appendix A. Supplementary material

Supplementary data to this article can be found online at https://doi.org/10.1016/j.ces.2019.08.001.

References

Akiyama, G., Matsuda, R., Sato, H., Hori, A., Takata, M., Kitagawa, S., 2012. Effect of functional groups in MIL-101 on water sorption behavior. Microporous Mesoporous Mater. 157, 89–93.
Aristov, Y.I., 2013. Challenging offers of material science for adsorption heat transformation: a review. Appl. Therm. Eng. 50, 1610–1618.
Bai, Y., Dou, Y., Xie, L.-H., Rutledge, W., Li, J.-R., Zhou, H.-C., 2016. Zr-based metal–organic frameworks: design, synthesis, structure, and applications. Chem. Soc. Rev. 45, 2327–2367.
Banerjee, D., Deibert, B.J., Wang, H., Li, J., 2011. Metal-organic frameworks: adsorption of hydrocarbons and alcohols. Encyclopedia Inorganic Bioinorg. Chemi., 1–21
Benjamin, T.E.O.H.W., Chakraborty, A., 2018. Aluminium Based Zeolites and MOFs for Adsorption Cooling. Transactions of the Japan Society of Refrigerating and Air Conditioning Engineers.
Berry, C., 2015. Residential Energy Consumption Survey. U.S. Energy Information Administration.
Chen, H., Chen, Z., Zhang, L., Li, P., Liu, J., Redfern, L.R., Moribe, S., Cui, Q., Snurr, R.Q., Farha, O.K., 2019. Toward design rules of metal-organic frameworks for adsorption cooling: effect of topology on the ethanol working capacity. Chem. Mater. 31, 2702–2706.
Clarke, L., Eom, J., Marten, E.H., Horowitz, R., Kyle, P., Link, R., Mignone, B.K., Mundra, A., Zhou, Y., 2018. Effects of long-term climate change on global building energy expenditures. Energy Econ. 72, 667–677.
de Lange, M.F., Verouden, K.J., Vlugt, T.J., Gascon, J., Kapteijn, F., 2015. Adsorption-driven heat pumps: the potential of metal–organic frameworks. Chem. Rev. 115, 12205–12250.
Demir, H., Mobedi, M., Ülkü, S., 2008. A review on adsorption heat pump: problems and solutions. Renew. Sustain. Energy Rev. 12, 2381–2403.
Dubbeldam, D., Calero, S., Ellis, D.E., Snurr, R.Q., 2016. RASPA: molecular simulation software for adsorption and diffusion in flexible nanoporous materials. Mol. Simul. 42, 81–101.
Erdős, M., de Lange, M.F., Kapteijn, F., Moultos, O.A., Vlugt, T.J.H., 2018. In silico screening of metal-organic frameworks for adsorption-driven heat pumps and chillers. ACS Appl. Mater. Interfaces 10, 27074–27087.
Glaznev, I., Ovoshchnikov, D., Aristov, Y.I., 2009. Kinetics of water adsorption/desorption under isobaric stages of adsorption heat transformers: the effect of isobar shape. Int. J. Heat Mass Transf. 52, 1774–1777.
Hafner, J., 2008. Ab-initio simulations of materials using VASP: Density-functional theory and beyond. J. Comput. Chem. 29, 2044–2078.
Henning, H.-M., 2007. Solar assisted air conditioning of buildings–an overview. Appl. Therm. Eng. 27, 1734–1749.
Henninger, S.K., Habib, H.A., Janiak, C., 2009. MOFs as adsorbents for low temperature heating and cooling applications. J. Am. Chem. Soc. 131, 2776–2777.
Henninger, S.K., Jeremias, F., Kummer, H., Schossig, P., Henning, H.-M., 2012. Novel sorption materials for solar heating and cooling. Energy Proc. 30, 279–288.
Jeremias, F., Lozan, V., Henninger, S.K., Janiak, C., 2013. Programming MOFs for water sorption: amino-functionalized MIL-125 and UiO-66 for heat transformation and heat storage applications. Dalton Trans. 42, 15967–15973.
Khutia, A., Rammelberg, H.U., Schmidt, T., Henninger, S., Janiak, C., 2013. Water sorption cycle measurements on functionalized MIL-101Cr for heat transformation application. Chem. Mater. 25, 790–798.
Li, S., Chung, Y.G., Simon, C.M., Snurr, R.Q., 2017. High-throughput computational screening of multivariate metal-organic frameworks (MTV-MOFs) for CO_2 capture. J. Phys. Chem. Lett. 8, 6135–6141.
Li, W., Li, S., 2018. CO_2 adsorption performance of functionalized metal-organic frameworks of varying topologies by molecular simulations. Chem. Eng. Sci. 189, 65–74.
Li, W., Xia, X., Cao, M., Li, S., 2019. Structure–property relationship of metal–organic frameworks for alcohol-based adsorption-driven heat pumps via high-throughput computational screening. J. Mater. Chem. A 7, 7470–7479.
Lin, C.-K., Zhao, D., Gao, W.-Y., Yang, Z., Ye, J., Xu, T., Ge, Q., Ma, S., Liu, D.-J., 2012. Tunability of band gaps in metal–organic frameworks. Inorg. Chem. 51, 9039–9044.
Majer, V., Svoboda, V., Kehiaian, H.V., 1985. Enthalpies of Vaporization of Organic Compounds: A Critical Review and Data Compilation. Blackwell Scientific, Oxford, pp. 104–109.
Nalaparaju, A., Zhao, X., Jiang, A.J., 2010. Molecular understanding for the adsorption of water and alcohols in hydrophilic and hydrophobic zeolitic metal– organic frameworks. J. Phys. Chem. C 114, 11542–11550.
Okunev, B., Gromov, A., Aristov, Y.I., 2013. Modelling of isobaric stages of adsorption cooling cycle: an optimal shape of adsorption isobar. Appl. Therm. Eng. 53, 89–95.
Potoff, J.J., Siepmann, J.I., 2001. Vapor–liquid equilibria of mixtures containing alkanes, carbon dioxide, and nitrogen. AIChE J. 47, 1676–1682.
Rappé, A.K., Casewit, C.J., Colwell, K., Goddard III, W.A., Skiff, W., 1992. UFF, a full periodic table force field for molecular mechanics and molecular dynamics simulations. J. Am. Chem. Soc. 114, 10024–10035.
Rezk, A., Al-Dadah, R., Mahmoud, S., Elsayed, A., 2013. Investigation of ethanol/metal organic frameworks for low temperature adsorption cooling applications. Appl. Energy 112, 1025–1031.
Segall, M., Linda, P., Probert, M., Pickard, C., Hasnip, P., Clark, S., Payne, M., 2002. Materials studio CASTEP, version 2.2. Accelrys, San Diego, CA.

Serre, C., 2012. Superhydrophobicity in highly fluorinated porous metal–organic frameworks. Angew. Chem. Int. Ed. 51, 6048–6050.
Sumida, K., Rogow, D.L., Mason, J.A., McDonald, T.M., Bloch, E.D., Herm, Z.R., Bae, T.-H., Long, J.R., 2011. Carbon dioxide capture in metal–organic frameworks. Chem. Rev. 112, 724–781.
Wade, C.R., Corrales-Sanchez, T., Narayan, T.C., Dincă, M., 2013. Postsynthetic tuning of hydrophilicity in pyrazolate MOFs to modulate water adsorption properties. Energy Environ. Sci. 6, 2172–2177.
Wang, C.-H., Bai, P., Siepmann, J.I., Clark, A.E., 2014. Deconstructing hydrogen-bond networks in confined nanoporous materials: implications for alcohol-water separation. J. Phys. Chem. C 118, 19723–19732.
Willems, T.F., Rycroft, C.H., Kazi, M., Meza, J.C., Haranczyk, M., 2012. Algorithms and tools for high-throughput geometry-based analysis of crystalline porous materials. Microporous Mesoporous Mater. 149, 134–141.
Zhou, H.-C., Long, J.R., Yaghi, O.M., 2012. Introduction to metal–organic frameworks. Chem. Rev. 112, 673–674.